ACTA IMEKO
ISSN: 2221-870X
*December 2026, Volume 15, Number 4, 1 - **9***

Assessment of natural radioactivity content, radiological hazard, ^{222}Rn exhalation rate, and mineralogical composition of Lipari Pumice stone (Sicily, Southern Italy): A case study

Lorenzo Pistorino[1], Francesco Caridi[1], Giuseppe Paladini[1], Antonio Francesco Mottese[2], Giuliana Faggio[2], Giacomo Messina[2], Francesco Gregorio[1], Domenico Majolino[1], Valentina Venuti[1]

[1] *Dipartimento di Scienze Matematiche e Informatiche, Scienze Fisiche e Scienze della Terra, Università degli Studi di Messina, V.le F. Stagno D'Alcontres, 31-98166 Messina, Italy*
[2] *Dipartimento di Ingegneria dell'Informazione, delle Infrastrutture e dell'Energia Sostenibile (DIIES), Università "Mediterranea", Via Zehender, 89122 Reggio Calabria, Italy*

ABSTRACT
This study investigates natural radioactivity, radiological hazard indices, radon exhalation, and the elemental and mineralogical composition of pumice from Lipari Island (Sicily, Italy), historically used as a building material. Activity concentrations of ^{226}Ra, ^{232}Th, and ^{40}K were measured using high-purity germanium (HPGe) gamma-ray spectrometry. The absorbed dose rate (D), annual effective dose equivalent ($AEDE$), activity concentration index (I_γ), and alpha index (I_α) were calculated to assess potential radiological implications. Although I_α remained below the adopted reference value, the other indicators exceeded their respective reference criteria, suggesting potential limitations on its use in construction.
Radon exhalation was measured using the closed chamber method coupled with a Durridge RAD8 detector. The material's contribution to indoor radon activity concentration was estimated using the Markkanen room model. The predicted concentration of 0.43 Bq m^{-3} indicates a limited contribution under the assumed exposure and ventilation conditions.
Complementary X-ray fluorescence (XRF) and X-ray diffraction (XRD) analyses characterized the elemental composition and mineralogical features, supporting the interpretation of radionuclide occurrence within the pumice matrix.
By integrating radionuclide measurements, radiological indices, experimental radon exhalation data, and indoor radon modelling, this study extends previous investigations of Lipari pumice and Italian building materials, providing evidence to inform the radiological assessment of volcanic materials used in construction.

Section: RESEARCH PAPER

Keywords: Lipari pumice; building materials; natural radioactivity; radiological health hazard; radon exhalation; Markkanen room model; mineralogy

Citation: L. Pistorino, F. Caridi, G. Paladini, A. F. Mottese, G. Faggio, G. Messina, F. Gregorio, D. Majolino, V. Venuti , Assessment of natural radioactivity content, radiological hazard, ^{222}Rn exhalation rate, and mineralogical composition of Lipari Pumice stone (Sicily, Southern Italy): A case study, Acta IMEKO, vol. 15 (2026) no. 4, pp. 1-9. DOI: 10.21014/actaimeko.v15i4.2347

Section Editor: Fabio Leccese, Università Degli Studi Roma Tre, Rome, Italy

Received March 18, 2026; **In final form** November 19, 2026; **Published** December 2026

Copyright: This is an open-access article distributed under the terms of the Creative Commons Attribution 4.0 International License.

Corresponding authors: Lorenzo Pistorino, e-mail: lorenzo.pistorino@studenti.unime.it; Francesco Caridi, e-mail: fcaridi@unime.it

1. INTRODUCTION

Human exposure to ionizing radiation originates from both natural—including primordial and cosmogenic radionuclides—and anthropogenic sources [1]. Primordial radionuclides, notably those belonging to the decay chains of ^{238}U, ^{232}Th, and ^{235}U, have been present in the Earth's crust since its formation. Their distribution is primarily controlled by geological setting, mineralogical composition, and tectonic evolution, leading to significant spatial variability in terrestrial radiation levels worldwide. In contrast, exposure to cosmogenic radionuclides depends on parameters such as altitude, latitude, and atmospheric conditions, all of which influence cosmic ray intensity and radionuclide production rates.

Artificial radioactivity, on the other hand, derives from radionuclides such as ^{239}Pu, ^{137}Cs, and ^{131}I, which are mainly generated by human activities, including nuclear power production, nuclear accidents, medical applications, and various industrial processes.

Among the principal contributors to indoor radiation exposure are natural stones, widely employed as building

materials. Owing to their extensive use in construction, both for structural purposes and decorative applications, the radioactivity content of these materials has increasingly become a subject of international research interest [2]. This attention arises from the presence of Naturally Occurring Radioactive Materials (NORMs), which may lead to two main exposure mechanisms: external exposure due to gamma radiation emitted by the materials themselves, and internal exposure resulting from inhalation of radon gas (^{222}Rn) and its short-lived alpha-emitting progeny, such as ^{218}Po and ^{214}Po.

In the present work, a multi-analytical approach was adopted to investigate both the radioactivity content and the elemental and mineralogical characteristics of a pumice sample collected on Lipari Island (Sicily, Southern Italy). Activity concentrations of ^{226}Ra, ^{232}Th, and ^{40}K were determined by means of High-Purity Germanium (HPGe) gamma-ray spectrometry. Subsequently, several radiological hazard indices—namely, the absorbed gamma dose rate (D), the Annual Effective Dose Equivalent ($AEDE$), the activity concentration index (I_γ), and the alpha index (I_α)—were calculated in order to evaluate potential hazards associated with long-term exposure to the investigated material.

Radon exhalation from the investigated material was assessed using the Closed Chamber Method (CCM) coupled with a Durridge RAD8 radon detector system [3]–[4]. To further evaluate the potential implications for indoor air quality, the measured exhalation rates were subsequently implemented in the Markkanen room model [5], a widely adopted approach for estimating indoor radon concentration as a function of surface exhalation, room volume, air exchange rate, and radon decay constant. This modelling step enabled a realistic assessment of the potential indoor radon levels associated with the use of the investigated material, and allowed a direct comparison with the national reference limits established by Legislative Decree 101/2020 [6], thereby providing a more reliable radiological hazard evaluation.

Within this framework, Lipari pumice has historically been employed in construction applications—particularly for lightweight concrete production, paving, and architectural elements—owing to its favourable physical and mechanical properties [7].

Specifically, previous studies on volcanic stones, tuff, pumice, and other Italian building materials have examined elemental composition, mechanical performance, and durability [8]–[9]. Complementing earlier radiometric investigations of Lipari pumice [10], the present study provides, to our knowledge, the first integrated assessment of its potential radiological hazard as a building material, combining the evaluation of external gamma exposure with experimental radon exhalation measurements and indoor radon modelling.

2. GEOLOGICAL FRAMEWORK

Lipari is the largest island of the Aeolian Archipelago, a volcanic island arc located in the southern Tyrrhenian Sea, north of Sicily (Italy). The Aeolian Islands constitute an active volcanic arc, related to the subduction of the Ionian lithosphere beneath the Calabrian Arc within the central Mediterranean convergent margin [11]–[13]. This geodynamic setting generates calc-alkaline to shoshonitic magmatism typical of subduction-related volcanic provinces, and is controlled by complex processes including slab rollback, mantle wedge metasomatism, and crustal magma differentiation [11]–[14].

Volcanic activity on Lipari started approximately 267 ka and has continued intermittently until historical times, producing a wide range of volcanic products from basaltic andesite to rhyolite [15]–[16]. The island is mainly composed of lava domes, pyroclastic deposits, pumice fallout layers, and obsidian lava flows, reflecting repeated cycles of explosive silicic volcanism followed by effusive activity [15]–[17]. Several eruptive centers developed through time, progressively building the island through overlapping volcanic units that record a complex stratigraphic and structural evolution [16].

The youngest volcanic activity is concentrated in the northeastern sector of Lipari, where the Monte Pilato pumice cone and the Rocche Rosse obsidian lava flow represent the most recent eruptive products of the island [18]. This eruptive sequence is generally attributed to a historical eruption dated between 1220 and 1230 AD, during which a highly explosive phase produced extensive rhyolitic pumice fallout deposits, subsequently followed by the emplacement of viscous obsidian lava flows [18].

The Monte Pilato deposits consist predominantly of highly vesicular rhyolitic pumice generated during Plinian to sub-Plinian explosive activity. These deposits form thick pyroclastic accumulations widely exposed along the northeastern coastal sector of the island, and represent one of the most significant pumice resources in the Mediterranean area, historically exploited for industrial and construction purposes [7].

From a petrological perspective, Lipari volcanic products belong to an evolved calc-alkaline magmatic series typical of subduction-related volcanic arcs [11]–[14]. The rhyolitic compositions characterizing the Monte Pilato pumice are interpreted as the result of advanced magmatic differentiation processes involving fractional crystallization, magma mixing, and crustal contamination within shallow magma reservoirs [15].

Mineralogically, Lipari pumice is largely composed of volcanic glass with minor crystalline phases, such as sanidine, plagioclase, and Fe–Ti oxides, reflecting rapid quenching of silica-rich magma during explosive eruptions [15]–[16].

These geological and petrological characteristics provide an important framework for interpreting the elemental composition and natural radioactivity investigated in the present study.

3. MATERIALS AND METHODS

3.1. Sampling

The pumice sample investigated in this study was collected from a currently inactive quarry located along Provincial Road No. 180 in Porticello. Together with Acquacalda, Porticello forms part of the historical pumice-quarrying district associated with the Monte Pilato volcanic centre, where pumice was extracted for use as a building material.

As widely reported in the literature [19]–[21], five aliquots of the material were collected and stored in properly labelled plastic containers, in order to avoid contamination during handling and transport. GPS coordinates of the sampling site are 38° 30' 35.1" N and 14° 57' 43.4" E. The limitations of this sampling strategy in terms of representativeness are discussed in Section 6 (*Limitations of the study*).

The location of the sampling site within Lipari Island and the geological map of the investigated area are shown in Figure 1.

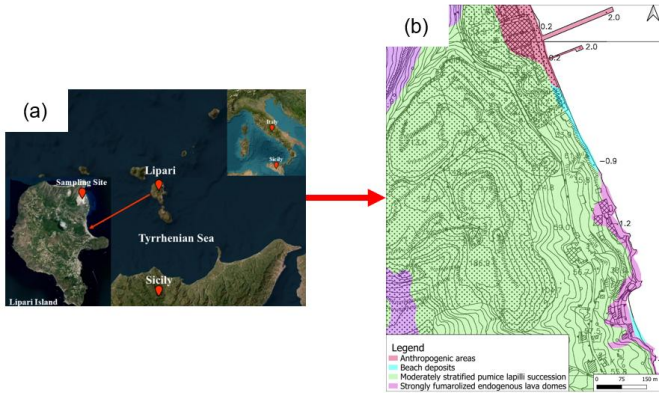

Figure 1. (a) Geographic location of the sampling site on Lipari Island (Aeolian Archipelago, southern Tyrrhenian Sea, Italy); (b) Geological map of the investigated area (scale 1:5000) showing the distribution of the main lithological units.

3.2. HPGe gamma spectrometry

Prior to HPGe gamma spectrometric analysis, each aliquot was oven-dried at 105 °C and subsequently ground using a vibratory micro-mill in order to obtain a homogeneous fine powder. The resulting material was then sieved to achieve a particle size smaller than 2 mm and transferred into hermetically sealed 250 mL Marinelli beakers. To allow the establishment of secular equilibrium between ^{226}Ra and its short-lived progeny, the sealed samples were stored for 30 days before measurement. Gamma spectra were acquired over a counting live time of 70,000 s, and radionuclide activity concentrations were determined from their characteristic gamma emissions. In particular, the activity concentration of ^{226}Ra was evaluated using the γ-lines at 295.21 keV and 351.92 keV emitted by ^{214}Pb, together with the 1120.29 keV emission of ^{214}Bi. The activity concentration of ^{232}Th was determined from the γ-lines of ^{228}Ac at 911.21 keV and 968.97 keV, while ^{40}K activity concentration was calculated from its characteristic emission line at 1460.8 keV [22].

Gamma spectrometric measurements were performed using an electrically cooled, direct-biased HPGe GEM detector manufactured by Ortec (Oak Ridge, TN, USA), installed within a lead shielding assembly to reduce background radiation contributions. The detector provides a full width at half maximum (FWHM) resolution of 1.85 keV, a relative efficiency of 40 %, and a peak-to-Compton ratio of 64:1, thereby ensuring high spectral resolution. Energy and efficiency calibrations were carried out using a traceable multi-nuclide standard source (Eckert & Ziegler Nuclitec GmbH, Berlin, Germany; reference BC4464), covering the energy interval from 59.54 keV to 1836.09 keV. The calibration source reproduced the same measurement geometry as the samples, and consisted of radionuclides embedded in an epoxy resin matrix with water-equivalent density. Spectral acquisition and data processing were conducted using Ortec GammaVision software [23].

Laboratory background peaks were accounted for using the software's peaked-background correction, based on a background measurement performed using ultrapure water in a Marinelli beaker matching the sample measurement geometry [24]. The background peak count rates were scaled to the sample live time and subtracted from the corresponding sample peak areas, with the associated uncertainties included in the counting uncertainty. Minimum detectable activity concentrations (MDAs) were calculated using the RISO method implemented in the GammaVision software. For the aliquot documented in the analytical report, the MDAs were 1.73, 1.63, 3.02, and 9.32 Bq kg^{-1} dry weight (d.w.) for ^{214}Pb, ^{214}Bi, ^{228}Ac, and ^{40}K, respectively.

Total measurement uncertainties were calculated in GammaVision by combining the relevant uncertainty contributions in quadrature. These included counting statistics, with the contribution from peaked-background subtraction, efficiency calibration uncertainty, and additional contributions associated with calibration-source uncertainty, repeatability, instrumental response variability, and sample filling geometry. Total uncertainties were reported at the two-sigma level, corresponding to a coverage factor of (k = 2), consistent with the uncertainty treatment described [25].

Quality assurance was supported by calibration with a traceable multi-nuclide standard source. Published validation of the gamma-spectrometric methodology at the same laboratory included the assessment of linearity, repeatability, accuracy, trueness, and detection limits using IAEA-certified reference materials [26].

The activity concentration of each detected radionuclide, expressed in Bq kg^{-1} dry weight (d.w.), was calculated according to the following equation [27]:

$$C\ (\mathrm{Bq\ kg^{-1}}) = \frac{N_E}{\varepsilon_E\ t\ \gamma_\mathrm{d}\ M}, \tag{1}$$

where N_E and ε_E are the net area of the peak at energy E and the calibration efficiency at energy E, respectively, while t is the acquisition live time (in s), γ_d is the gamma emission probability and M is the dry mass of the analyzed sample (in kg).

The accuracy and reliability of the gamma spectrometric measurements are certified by the Italian Accreditation Body (ACCREDIA) [28].

3.3. Radiological health hazard

The radiological health hazard was initially assessed by calculating the absorbed gamma dose rate, D (nGy h^{-1}), for indoor external exposure according to the standard room model [29]:

$$D = 0.92\ C_\mathrm{Ra} + 1.1\ C_\mathrm{Th} + 0.08\ C_\mathrm{K}, \tag{2}$$

where C_Ra, C_Th, and C_K are the average specific activities of ^{226}Ra, ^{232}Th, and ^{40}K, respectively.

The Annual Effective Dose Equivalent, $AEDE$ (in mSv y^{-1}), for indoor external exposure was subsequently calculated using the following relationship [29]–[30]:

$$AEDE = (D - 50) \cdot 8760\ \mathrm{h} \cdot 0.7\ \mathrm{Sv\ Gy^{-1}} \cdot 0.8 \cdot 10^{-6}, \tag{3}$$

where the worldwide average background dose rate of 50 nGy h^{-1} was subtracted, 0.7 Sv Gy^{-1} represents the dose conversion coefficient, and the occupancy factor of 0.8 accounts for the average fraction of time spent indoors. According to current regulations, the $AEDE$ value should not exceed 1 mSv y^{-1} in order to ensure negligible radiological hazard [6].

The following equation was used to determine the Activity Concentration Index (I_γ) [31]:

$$I_\gamma = \frac{C_\mathrm{Ra}}{300} + \frac{C_\mathrm{Th}}{200} + \frac{C_\mathrm{K}}{3000}. \tag{4}$$

This index is commonly used as a screening parameter to identify building materials that may present a radiological concern when employed in construction. Materials characterized

by $I_\gamma > 1$ should generally be avoided, as they may lead to annual dose values > 1 mSv y^{-1}, thus exceeding the recommended safety threshold.

Finally, the alpha index is used to evaluate the additional alpha radiation exposure resulting from radon inhalation originating from building materials [32]:

$$I_\alpha = \frac{C_{\mathrm{Ra}}}{200}. \tag{5}$$

In detail, to ensure that indoor radon concentrations remain below the recommended reference value of 200 Bq m^{-3}, the ^{226}Ra activity concentration in building materials must not exceed 200 Bq kg^{-1}, as set by Italian Legislation [6]. Therefore, for radiation exposure to be considered negligible in terms of radiological hazard, $\boldsymbol{I_\alpha}$ must not exceed the threshold value of 1.

3.4. ^{222}Rn exhalation rate

Radon exhalation rate measurement was performed using the Closed Chamber Method (CCM) [4] coupled with a Durridge RAD8 system (Durridge Co., Billerica, MA, USA), a portable continuous radon monitor based on solid-state alpha spectrometry [33] Specifically, the instrument determines the activity concentration of ^{222}Rn in air by detecting alpha emissions from its short-lived decay products, primarily ^{218}Po and ^{214}Po, which are electrostatically collected within the internal detection chamber.

The experimental setup consisted of a 2.8 L airtight accumulation chamber connected to the RAD8 inlet and outlet ports through sealed tubing, thereby forming a closed-loop air circulation system. The circuit incorporated a drying unit filled with $CaSO_4$ desiccant to reduce humidity levels and improve measurement stability, as well as an in-line particulate filter to prevent dust and radon progeny from entering the detector. A photograph of the experimental setup is shown in Figure 2.

During measurements, the internal pump of the instrument ensured continuous air circulation within the closed-loop system, allowing a homogeneous radon distribution and the establishment of radon–progeny equilibrium within 15–20 minutes [34] Prior to each test, routine background checks and system integrity controls were carried out to minimize potential interferences related to residual radon, humidity, and leakage effects.

The radon exhalation behaviour of the investigated sample was evaluated by modelling the temporal increase of ^{222}Rn activity concentration inside the closed chamber. Assuming a constant radon release rate from the sample into a sealed volume and neglecting external air exchange, the evolution of radon concentration in the chamber can be described by the following first-order mass balance equation [35]:

$$\frac{\mathrm{d}C}{\mathrm{d}t} = \frac{E}{V} - \lambda_{\mathrm{eff}}\, C\,, \tag{6}$$

where C is the ^{222}Rn activity concentration (in Bq m^{-3}), E is the total radon exhalation rate (in Bq h^{-1}), V is the free total volume of the chamber (in m^3) and λ_{eff} is the effective radon decay constant (in h^{-1}) which accounts for the physical ^{222}Rn radioactive decay (λ_{222}) and possible additional losses due to back-diffusion or leakage effects from the chamber [34]–[35]:

$$\lambda_{\mathrm{eff}} = \lambda_{222} + \lambda_{\mathrm{leak}} + \lambda_{\mathrm{back}}\,. \tag{7}$$

By integrating equation (6) with the initial condition $C(t=0) = C_0$, the radon accumulation curve can be expressed as:

$$C = C_0\, \mathrm{e}^{-\lambda_{\mathrm{eff}}\, t} + \frac{E}{\lambda_{\mathrm{eff}}\, V}\left(1 - \mathrm{e}^{-\lambda_{\mathrm{eff}}\, t}\right), \tag{8}$$

in which C_0 is the initial radon concentration in the system. Specifically, the first term represents the decay of any residual radon initially present in the closed-loop circuit, while the second term describes the progressive radon build-up towards equilibrium conditions.

Finally, the radon exhalation rate E was calculated using the following equation [36]:

$$E = \frac{\left(C - C_0\, \mathrm{e}^{-\lambda_{\mathrm{eff}}\, T}\right)}{1 - \mathrm{e}^{-\lambda_{\mathrm{eff}}\, T}}\, \lambda_{\mathrm{eff}}\, V\,, \tag{9}$$

where C refers to the equilibrium radon concentration, V is the free total volume of the analytical system (in m^3), and T = 245 h is the exposure time.

To further evaluate the potential impact of the investigated material on indoor air quality, the Markkanen room model was employed [5]. The model describes the time-dependent accumulation of radon in an enclosed standard room by means of a mass-balance approach that accounts for radon exhalation from building materials, radioactive decay of ^{222}Rn, and air exchange due to ventilation.

Specifically, the mass balance equation for the indoor radon concentration $C(t)$ can be written as:

$$\frac{\mathrm{d}C(t)}{\mathrm{d}t} = \frac{J \cdot A}{V} - \left(\lambda_{222} + \frac{1}{\tau}\right) C(t), \tag{10}$$

where J is the specific radon exhalation rate (in Bq h^{-1} m^{-2}), A is the effective exhaling surface area (in m^2), V is the room volume (in m^3), λ_{222} is the decay constant of ^{222}Rn (in h^{-1}), and τ is the air exchange time (in h), related to the ventilation rate.

The analytical solution of equation (10) provides the time evolution of indoor radon concentration:

$$C(t) = C_\infty \left[1 - \mathrm{e}^{-\left(\lambda_{222} + \frac{1}{\tau}\right) t}\right], \tag{11}$$

in which C_∞ represents the equilibrium indoor radon concentration, given by:

$$C_\infty = \frac{J \cdot A}{V\left(\lambda_{222} + \frac{1}{\tau}\right)}. \tag{12}$$

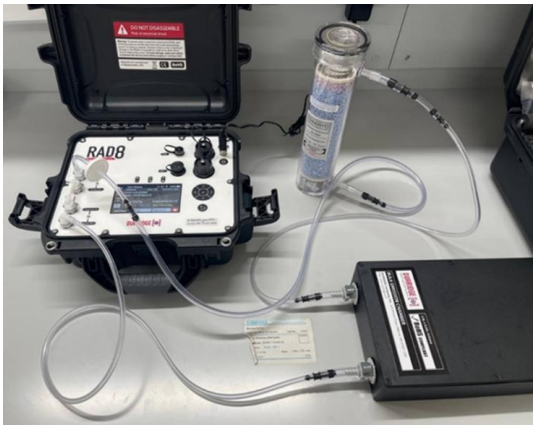

Figure 2. Experimental set-up of the Durridge RAD8 for the radon exhalation assessment.

For the present study, simulations were carried out assuming a standard room geometry (4 m × 5 m × 2.8 m), a minimum ventilation rate of 0.2 h^{-1}, uniform radon distribution within the indoor volume, and absence of additional radon sources. These assumptions were selected to represent an extremely conservative indoor exposure scenario.

3.5. X-ray Fluorescence (XRF)

Elemental composition was determined using a portable XRF analyzer (Alpha 4000, Innov-X Systems, Woburn, MA, USA) equipped with a tantalum anode X-ray tube and a silicon PIN diode detector featuring an active area of 170 mm^2 and an energy resolution better than 220 eV at 5.95 keV. The instrument allows the detection of elements with atomic numbers ranging from 15 (P) to 82 (Pb).

Measurements were performed in 'soil' analytical mode, employing Compton normalization to improve trace element detection in the ppm concentration range. The selected 'Environmental' element suite enabled simultaneous analysis of a wide range of elements, including P, S, Cl, K, Ca, Fe, and Pb. Each sample was measured through two consecutive acquisition cycles conducted at 40 kV/7 μA and 15 kV/5 μA, respectively, resulting in a total acquisition time of 120 s per analysis.

Instrument control and data acquisition were managed using an HP iPAQ Pocket PC. Calibration procedures were performed through the LEAP II software and validated using certified reference materials. The spectral peaks observed at approximately 8.15 keV and 9.34 keV correspond to the L_α and L_β characteristic emissions of the tantalum anode.

3.6. X-ray Diffraction (XRD)

X-ray Diffraction (XRD) measurements were carried out using a Malvern PANalytical Empyrean diffractometer (Malvern, UK) equipped with a Cu K_α radiation source operating in Bragg–Brentano θ-θ geometry and coupled with a PIXcel solid-state detector [37]. For each aliquot, approximately 1 g of pumice material was finely ground prior to analysis, in order to obtain a homogeneous powder suitable for diffraction measurements.

The diffractometer was operated at 40 kV and 40 mA. Diffraction patterns were recorded over a 2θ angular range from 2 ° to 70 °, using a step size of 0.053 ° and a counting time of 4.08 s per step.

Post-acquisition data processing involved removal of the Cu $K_{\alpha 2}$ component using HighScore Plus software (version 5.1), followed by background reduction through digital filtering procedures. Mineral phases present in the powdered pumice were identified by comparing the measured diffraction peak positions with reference patterns contained in the ICDD JCPDS database [38].

4. RESULTS AND DISCUSSION

Table 1 presents the average activity concentrations of ^{226}Ra, ^{232}Th, and ^{40}K measured in the investigated pumice sample, as assessed from the five analyzed aliquots.

The obtained values clearly exceed the worldwide mean activity concentrations of 35 Bq kg^{-1}, 30 Bq kg^{-1}, and 400 Bq kg^{-1} for ^{226}Ra, ^{232}Th, and ^{40}K, respectively [30]. A more comprehensive interpretation of these relatively high levels can be achieved by integrating the radiometric results with the elemental and mineralogical evidence discussed in the following sections.

Table 1. Mean activity concentrations of ^{226}Ra, ^{232}Th, and ^{40}K in the analyzed natural stone.

Sample	^{226}Ra (Bq kg^{-1} d.w.)	^{232}Th (Bq kg^{-1} d.w.)	^{40}K (Bq kg^{-1} d.w.)
Lipari pumice	179 ± 21	203 ± 25	1262 ± 135

Table 2. Activity concentration comparison (Bq kg^{-1} dry weight) between Lipari pumice and selected natural building materials.

Sample	^{226}Ra (Bq kg^{-1} d.w.)	^{232}Th (Bq kg^{-1} d.w.)	^{40}K (Bq kg^{-1} d.w.)	Reference
Lipari pumice	179 ± 21	203 ± 25	1262 ± 135	This work
Red granite	20.1 ± 2.8	42.8 ± 5.9	1071 ± 127	[39]
Basalt	41.3 ± 5.1	53.1 ± 6.9	157 ± 19	[39]
Tuff	50.7	58.6	717.6	[40]

In detail, for comparison purposes, Table 2 reports literature data for other natural stones widely used in the construction sector, including red granite, basalt, and tuff, alongside the values measured for Lipari pumice.

Specifically, the data indicate that Lipari pumice exhibits substantially higher ^{226}Ra and ^{232}Th activity concentrations than those typically reported for common construction stones. Such enrichment in naturally occurring radionuclides points to a potentially higher radiological relevance when this material is employed in building applications.

The calculated radiological parameters—D, $AEDE$, I_γ, and I_α—obtained using equations (2)–(5) are summarized in Table 3.

The relatively high D value, when compared with the world average background value of 50 nGy h^{-1}, is mainly related to the intrinsic lithological features of the sampling area [41].

In addition, although the estimated $AEDE$ exceeds the regulatory reference value of 1 mSv y^{-1} established by Italian legislation [6], it should be noted that this estimate is based on an extremely conservative exposure scenario assuming continuous indoor occupancy (8760 h y^{-1}).

Similarly, the I_γ index was found to be greater than unity, suggesting that the use of this material in construction may require careful radiological evaluation. These findings support the need for more detailed, application-specific dose assessments when natural stones are intended for civil engineering purposes, particularly in residential settings and buildings characterized by high occupancy factors. This approach is consistent with the provisions of Article 29, paragraph 5, of Italian Legislative Decree 101/2020 [6], implementing EU Directive 2013/59/Euratom [42] on fundamental radiation protection standards. Such assessments should be performed using recognized national and international methodologies, taking into account parameters such as material density, thickness, building typology, and intended end use.

In contrast, the calculated alpha index (I_α) was found to be equal to 0.9, thus remaining below the recommended limit value of 1.

In addition to external gamma exposure, the potential radiological impact associated with the investigated material was further examined in terms of radon release behaviour. In this

Table 3. Radiological hazard parameters for the analyzed sample: absorbed dose rate (*D*), Annual Effective Dose Equivalent (*AEDE*), activity concentration index (I_γ), and alpha index (I_α).

Sample	*D* (nGy h^{-1})	*AEDE* (mSv y^{-1})	I_γ	I_α
Lipari pumice	489.1	2.2	2.0	0.9

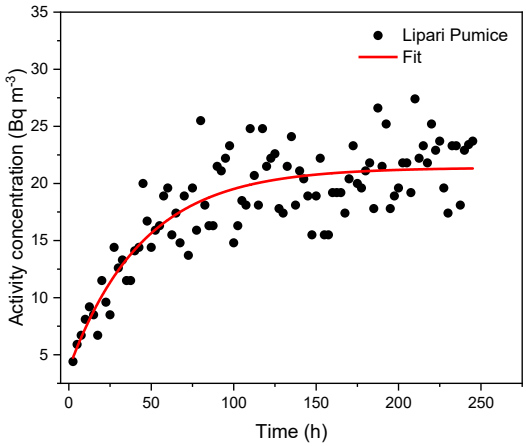

Figure 3. The most representative radon growth curve to equilibrium for the Lipari pumice stone.

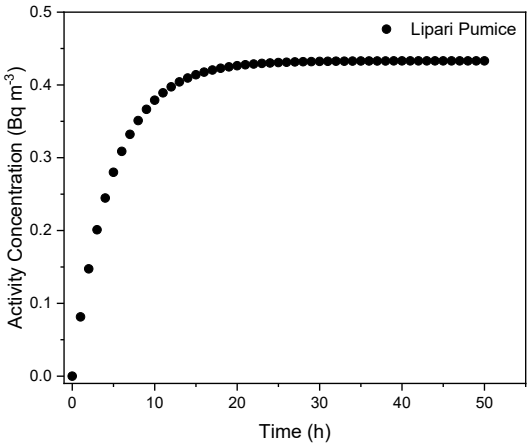

Figure 4. Radon accumulation growth curve simulated using the Markkanen room model under the most conservative conditions, i.e. adopting the measured radon exhalation rate, a standard room geometry (4 m × 5 m × 2.8 m), and a minimum ventilation rate of 0.2 h^{-1} for the investigated Lipari pumice.

context, experimental measurements of the radon exhalation rate were carried out in order to evaluate the contribution of the Lipari pumice to indoor radon levels.

Radon accumulation tests were therefore performed using the Closed Chamber Method (CCM) coupled with the RAD8 detection system, allowing the time-dependent growth of radon concentration within the accumulation volume to be monitored.

The resulting radon accumulation curve obtained for the Lipari pumice sample is presented in Figure 3.

Table 4 summarizes the radon exhalation rate (in Bq h^{-1}), the specific radon exhalation rate (in Bq h^{-1} m^{-2}), and the effective decay constant (in h^{-1}) obtained for the Lipari pumice sample.

The values reported in Table 4 indicate a relatively limited radon release from the investigated pumice. In particular, the measured radon exhalation rate is markedly lower than those previously reported for several natural stones widely used as building materials in Italy [36]. This behaviour suggests that, despite the elevated ^{226}Ra activity concentration, Lipari pumice exhibits a comparatively low radon release potential under the investigated experimental conditions.

Furthermore, a comparison between the effective decay constant ($\lambda_{\mathrm{eff}} = 0.022\ \mathrm{h}^{-1}$) and the physical decay constant of radon ($\lambda_{222} \simeq 0.008\ \mathrm{h}^{-1}$) confirms that additional loss mechanisms (i.e. back-diffusion and possible system leakage) contribute to the observed radon removal and must be considered in the growth curve modelling.

The potential indoor radon accumulation associated with the investigated material was further evaluated using the Markkanen room model. The simulated radon concentration trends derived from equations (11) and (12) are presented in Figure 4.

The simulated equilibrium indoor radon activity concentration obtained for the Lipari pumice was found to be 0.43 Bq m^{-3}, which is far below the reference levels established by Legislative Decree No. 101/2020. In particular, the Italian regulation sets a reference level of 300 Bq m^{-3} (annual average) for existing buildings and workplaces, and a more restrictive value of 200 Bq m^{-3} for new residential constructions [6].

In addition, the predicted concentration is also well below the reference level recommended by the World Health Organization (100 Bq m^{-3}) and the action level adopted by the U.S. Environmental Protection Agency (148 Bq m^{-3}) [43]–[44].

These results indicate that, under the investigated conditions, the contribution of Lipari pumice to indoor radon exposure can be considered negligible from a radiological protection perspective, and no specific mitigation actions (e.g. the application of consolidating agents) appear to be required.

Nevertheless, it should be noted that the present assessment is based on controlled laboratory conditions and simplified modelling assumptions. Factors such as ventilation variability, building design, material thickness, and long-term environmental conditions may influence actual indoor radon levels. Further investigations, including in situ measurements, would be beneficial to fully validate the present findings.

Going on, a representative XRF spectrum of the Lipari pumice sample, obtained from five independent measurements over the 0–40 keV energy range, is shown in Figure 5.

Table 4. The radon exhalation rate, the specific radon exhalation rate, and the effective decay constant obtained for the Lipari pumice sample.

Sample	E (Bq h^{-1})	Specific Radon Exhalation Rate (Bq h^{-1} m^{-2})	λ_{eff} (h^{-1})
Lipari pumice	$(1.32 \pm 0.12) \cdot 10^{-3}$	$(5.58 \pm 0.19) \cdot 10^{-2}$	0.022 ± 0.003

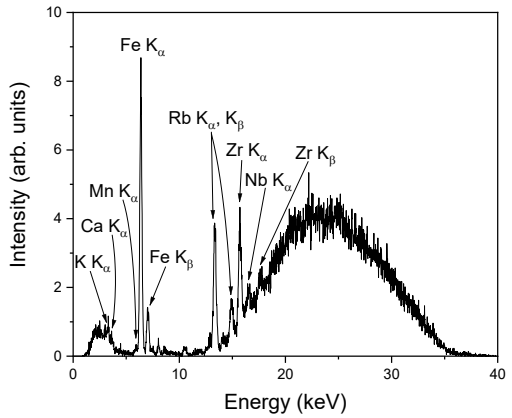

Figure 5. Representative XRF spectra recorded on the Lipari pumice natural stone, in the energy range between 0 and 40 keV.

In detail, XRF analysis revealed the presence of major elements, such as Fe, together with trace constituents including K, Mn, Ca, Rb, Zr, and Nb, confirming the volcanic origin of the material and its consistency with intermediate-felsic products typical of the Aeolian Arc [11]. The pronounced K peak observed in the spectrum is consistent with the elevated ^{40}K activity and can reasonably be attributed to K-bearing mineral phases, such as sanidine and/or orthoclase.

The occurrence of Rb is likely linked to magmatic differentiation processes, whereas High Field Strength Elements (HFSE), particularly Zr and Nb, represent key geochemical tracers of magma evolution and source characteristics [45], typically hosted in accessory mineral phases.

In this context, the presence of Zr- and Nb-bearing accessories (e.g. zircon and niobate minerals) may account for the relatively high activities measured for ^{232}Th and ^{226}Ra, given their well-known capacity to incorporate Th and U within their crystal structures. Moreover, Fe and Mn are plausibly associated with oxide phases and minor ferromagnesian components that may contribute, albeit secondarily, to the overall radioactivity of the sample.

Figure 6 displays the most representative XRD pattern of the analyzed pumice sample.

The diffraction pattern clearly emphasizes the predominantly glassy nature of the material. Specifically, the very low intensity of identifiable diffraction peaks, together with the presence of a broad amorphous halo in the 20 ° – 30 ° 2θ interval, supports the dominance of volcanic glass and indicates that any crystalline accessory phases occur at concentrations below the instrumental detection limit. The lack of well-defined crystalline reflections, accompanied only by weak and diffuse features, suggests a very limited crystalline fraction, consistent with rapid cooling following eruption. Indeed, fast quenching processes commonly generate glass-rich matrices, while preserving the bulk elemental signature of the parental melt.

In light of these observations, the apparent discrepancy between the elemental composition revealed by XRF (Figure 5) and the limited crystalline evidence provided by XRD (Figure 6) can be reasonably attributed to the largely amorphous nature of the pumice. Consequently, the elements identified by XRF (notably K, Zr, and Nb), which are associated with the measured radioactivity, are likely hosted either in cryptocrystalline accessory phases or incorporated in solid solution within the glassy matrix, as frequently reported for silicic pyroclastic materials [46]. Overall, the combined radiological, elemental, and mineralogical evidence—highlighting significant ^{232}Th, ^{226}Ra, and ^{40}K activity concentrations potentially linked to K-, Zr-, and Nb-bearing phases—supports the interpretation of the Lipari pumice as a typical product of evolved calc-alkaline magmatism in a subduction-related geodynamic context [14].

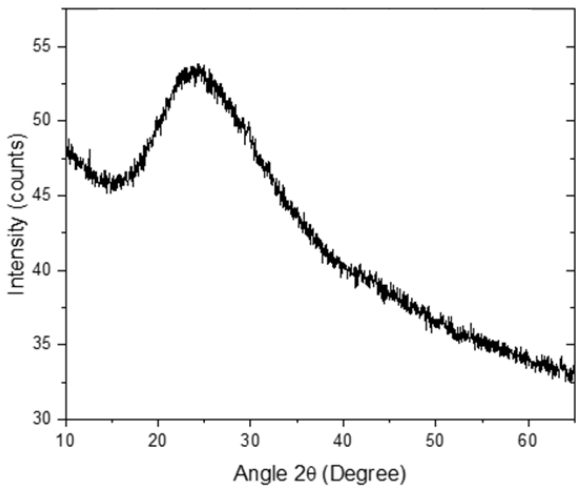

Figure 6. XRD spectrum of the Lipari pumice sample

5. CONCLUSIONS

The natural radioactivity content and radon exhalation rate of a pumice sample from Lipari (Sicily, Southern Italy) were investigated through HPGe gamma-ray spectrometry and the Closed Chamber Method with a Durridge RAD8 detector, respectively, and are reported as a case study.

HPGe gamma spectrometry measurements revealed activity concentrations of (179 ± 21) Bq kg^{-1}, (203 ± 25) Bq kg^{-1}, and (1262 ± 135) Bq kg^{-1} for ^{226}Ra, ^{232}Th, and ^{40}K, respectively, all exceeding the corresponding worldwide average values.

Then, the absorbed gamma dose rate (D), the Annual Effective Dose Equivalent ($AEDE$), the activity concentration index (I_γ), and the alpha index (I_α) were calculated in order to assess the potential radiological hazard associated with prolonged exposure to the investigated material, particularly in view of its widespread use as a building material. The obtained results showed that D, $AEDE$, and I_γ exceed the recommended reference values under the adopted conservative scenario, while only the alpha index ($I_\alpha = 0.9$) was found to be below the safety threshold.

Despite the relatively elevated ^{226}Ra activity concentration, the measured radon exhalation rate was found to be comparatively low with respect to other natural stones commonly employed in the Italian construction sector. This behaviour suggests a limited radon release capability of the Lipari pumice, likely related to partial radon retention within its predominantly glassy matrix.

Furthermore, the application of the Markkanen room model under conservative conditions yielded an equilibrium indoor radon concentration of 0.43 Bq m^{-3}, which is orders of magnitude below the reference levels established by Italian legislation (300 Bq m^{-3}) and by international guidelines. From the perspective of indoor radon exposure, the investigated pumice can therefore be considered to pose a negligible radiological hazard.

Finally, XRF spectroscopy and XRD analyses were employed to correlate the measured radioactivity content with the elemental and mineralogical properties of the investigated pumice. Specifically, XRF results highlighted the presence of K-, Zr-, and Nb-bearing components, while XRD confirmed the predominantly glassy nature of the material. The elevated radionuclide concentrations are therefore likely associated with accessory phases and solid solution within the volcanic glass matrix, consistent with evolved calc-alkaline magmatism in a subduction-related setting.

Overall, this work provides the first integrated radiological and mineralogical assessment of Lipari pumice, and contributes useful reference data for its safe and informed use in construction. Future studies, including in situ measurements, would be beneficial to further refine the radiological evaluation of this volcanic material.

6. LIMITATIONS OF THE STUDY

This case study is based on five aliquots collected at a single site in Porticello and characterizes the investigated sample only. Although Porticello and Acquacalda pumice-quarrying districts share the Monte Pilato geological context, radiological homogeneity has not been established. Future sampling will include additional locations, particularly Acquacalda, and different depths or stratigraphic levels.

The effects of porosity, pore connectivity, grain size, moisture content, sealing time, and possible glass-matrix retention on radon release were not systematically investigated. Moreover, qualitative XRF and the predominantly amorphous XRD pattern do not establish quantitative relationships between elemental composition, radionuclide activities, and hosting phases. Future work will include dedicated petrophysical and chemical–mineralogical characterization, including quantitative XRF with appropriate calibration standards.

Both exposure assessments adopted conservative scenarios for preliminary screening. External gamma exposure was estimated using the standard indoor room model for bulk material use, accounting for contributions from walls, floor, and ceiling, with $AEDE$ derived from background-corrected D using assumed occupancy and dose conversion factors. The Markkanen model combined low ventilation with an entirely emitting internal room surface; even under these conservative conditions, the predicted material contribution to indoor radon was only 0.43 Bq m^{-3}. These assumptions support a cautious assessment, although they do not establish an absolute upper bound for all building conditions. Material thickness effects on radon release were not independently characterized, application-specific assessments and in situ measurements are needed to refine both estimates.

REFERENCES

[1] D. Shahbazi-Gahrouei, M. Gholami, S. Setayandeh, A review on natural background radiation, Adv. Biomed. Res. 2 (2013) 1, pp. 65.
DOI: 10.4103/2277-9175.115821

[2] F. Caridi, D. Chiriu, S. Da Pelo, G. Faggio, M. Guida, G. Messina, M. Ponte, S. A. Ruffolo, (+ 2 more authors), Radon exhalation rate, radioactivity content, and mineralogy assessment of significant historical and artistic interest construction materials, Appl. Sci. 14 (2024) 23, pp. 11359.
DOI: 10.3390/app142311359

[3] L. Zhang, X. Lei, Q. Guo, S. Wang, X. Ma, Z. Shi, Accurate measurement of the radon exhalation rate of building materials using the closed chamber method, J. Radiol. Prot. 32 (2012) 3, pp. 315–323.
DOI: 10.1088/0952-4746/32/3/315

[4] P. Tuccimei, M. Castelluccio, M. Soligo, M. Moroni, Radon exhalation rates of building materials: experimental, analytical protocol and classification criteria, in: Building Materials: Properties, Performance and Applications. Nova Science Publishers, New York, 2009, pp. 259–273.

[5] M. Markkanen, Radiation Dose Assessments for Materials with Elevated Natural Radioactivity, Finnish Centre for Radiation and Nuclear Safety, Helsinki, 1995, ISBN 9517120796.

[6] Italian Government, Legislative Decree No. 101 of 31 July 2020. Online [Accessed 25 February 2026] https://www.normattiva.it/uri-res/N2Ls?urn:nir:stato:decreto.legislativo:2020-07-31;101

[7] G. Amato, G. Campione, L. Cavaleri, G. Minafò, M. Papia, La pomice per il confezionamento di calcestruzzi leggeri strutturali, Mecc. Mater. Strutt. 2 (2011) 1. [In Italian]

[8] G. Steinhauser, M. Bichler, G. Eigelsreiter, A. Tischner, Neutron activation analysis of pumice from Lipari, Italy, and the identification of a pumice find from the excavation at Tel Megadim, Israel, J. Radioanal. Nucl. Chem. 267 (2005) 1, pp. 3–8.
DOI: 10.1007/s10967-006-0001-4

[9] M. D. Jackson, F. Marra, R. L. Hay, C. Cawood, E. M. Winkler, The judicious selection and preservation of tuff and travertine building stone in ancient Rome, Archaeometry 47 (2005) 3, pp. 485-510.
DOI: 10.1111/j.1475-4754.2005.00215.x

[10] G. Lanzo, S. Basile, M. Brai, S. Rizzo, Volcanic products of Lipari (Aeolian islands, Italy): Multivariate analysis of petrographic and radiometric data, Radiat. Meas. 45 (2010) 7, pp. 816–822.
DOI: 10.1016/j.radmeas.2010.04.003

[11] A. Peccerillo, Plio-Quaternary Volcanism in Italy: Petrology, Geochemistry, Geodynamics, Springer, Berlin, 2005, ISBN 978-3-540-25885-0.

[12] G. De Astis, G. Ventura, G. Vilardo, Geodynamic significance of the Aeolian volcanism (Southern Tyrrhenian Sea, Italy) in light of structural, seismological, and geochemical data, Tectonics 22 (2003), pp. 1040.
DOI: 10.1029/2003TC001506

[13] J. Keller, The island of Salina, Rend. Soc. Ital. Mineral. Petrol. 36 (1980), pp. 489–524.

[14] R. M. Ellam, M. A. Menzies, C. J. Hawkesworth, W. P. Leeman, M. Rosi, G. Serri, The transition from calc-alkaline to potassic orogenic magmatism in the Aeolian Islands, southern Italy, Bull. Volcanol. 50 (1988), pp. 386–398.
DOI: 10.1007/BF01050638

[15] F. Forni, F. Lucchi, A. Peccerillo, C. A. Tranne, P. L. Rossi, M. L. Frezzotti, Stratigraphy and geological evolution of the Lipari volcanic complex (central Aeolian archipelago), in: F. Lucchi, A. Peccerillo, J. Keller, C. A. Tranne, P. L. Rossi (eds.), The Aeolian Islands Volcanoes, Geol. Soc. London Mem. 37 (2013), pp. 213–279.
DOI: 10.1144/M37.10

[16] F. Lucchi, C. A. Tranne, P. L. Rossi, Stratigraphic approach to geological mapping of the late Quaternary volcanic island of Lipari (Aeolian Archipelago, southern Italy), Geol. Soc. Am. Spec. Pap. 464 (2010).
DOI: 10.1130/2010.2464(01)

[17] R. De Rosa, H. Guillou, R. Mazzuoli, G. Ventura, New unspiked K-Ar ages of volcanic rocks of the central and western sector of the Aeolian Islands: reconstruction of the volcanic stages, J. Volcanol. Geotherm. Res. 120 (2003), pp. 161–178.
DOI: 10.1016/S0377-0273(02)00369-4

[18] M. Pistolesi, M. Rosi, A. B. Malaguti, F. Lucchi, C. Tranne, (+ 5 more authors), Chrono-stratigraphy of the youngest (last 1500 years) rhyolitic eruptions of Lipari (Aeolian Islands, Southern Italy) and implications for distal tephra correlations, J. Volcanol. Geotherm. Res. 420 (2021), pp. 107397.
DOI: 10.1016/j.jvolgeores.2021.107397

[19] J. Monnet, Soil and Rock Sampling Methods, John Wiley & Sons, Hoboken, 2015, ISBN 978-1-119-14561-5.

[20] F. Caridi, D. Chiriu, S. Da Pelo, G. Faggio, M. Guida, (+ 5 more authors), Natural radioactivity content, radon exhalation and mineralogical composition assessment of the Ignimbrite campana stone: a case study, Atti Accad. Pelorit. Pericol. Cl. Sci. Fis. Mat. Nat. 103 (2025) 2, A3.
DOI: 10.1478/AAPP.1032A3

[21] F. Caridi, G. Paladini, F. Gregorio, S. Lanza, G. Lando, M. Sfacteria, S. Tuccinardi, M. Venuti, P. Cardiano, D. Majolino, V. Venuti, Natural radioactivity content and radon exhalation rate assessment for building materials from the archaeological park of Tindari, Sicily, southern Italy: a case study, Int. J. Environ. Res. Public Health 22 (2025) 3, pp. 379.
DOI: 10.3390/ijerph22030379

[22] F. Caridi, A. F. Mottese, G. Paladini, L. Pistorino, F. Gregorio, S. Lanza, G. Randazzo, S. Marguccio, (+ 4 more authors), Multivariate statistics, radioactivity and radiological hazard

evaluation in marine sediments of selected areas from Sicily, southern Italy, J. Mar. Sci. Eng. 13 (2025) 4, pp. 769.
DOI: 10.3390/jmse13040769

[23] Ortec, GammaVision Software User Manual. Online [Accessed 13 March 2025]
https://www.ortec-online.com/products/software/gammavision

[24] F. Caridi, M. Di Bella, G. Sabatino, G. Belmusto, M. R. Fede, D. Romano, F. Italiano, A. F. Mottese, Assessment of natural radioactivity and radiological risks in river sediments from Calabria (Southern Italy), Appl. Sci. 11 (2021) 4, pp. 1729. DOI: 10.3390/app11041729

[25] F. Caridi, V. Venuti, G. Paladini, V. Crupi, G. Belmusto, D. Majolino, The radioactivity distribution and radiation hazard in honey samples from Italian large retailers, J. Phys.: Conf. Ser. 2162 (2022) 1, pp. 012002.
DOI: 10.1088/1742-6596/2162/1/012002

[26] F. Caridi, S. Marguccio, A. Belvedere, M. D'Agostino, Validation of gamma-ray spectrometry (GRS) for radionuclides analysis of environmental and food samples, SN Appl. Sci. 1 (2019), pp. 256. DOI: 10.1007/s42452-019-0267-0

[27] F. Caridi, G. Acri, A. Belvedere, V. Crupi, M. D'Agostino, S. Marguccio, M. Messina, G. Paladini, (+ 2 more authors), Evaluation of the radiological and chemical risk for public health from flour sample investigation, Appl. Sci. 11 (2021), pp. 3646.
DOI: 10.3390/app11083646

[28] ACCREDIA, Accredia. Online [Accessed 13 March 2025]
https://www.accredia.it/

[29] European Commission, Radiation Protection 112: Radiological Protection Principles Concerning the Natural Radioactivity of Building Materials, Directorate-General Environment, Luxembourg, 1999.

[30] UNSCEAR, Sources and Effects of Ionizing Radiation, United Nations Scientific Committee on the Effects of Atomic Radiation, United Nations, New York, 2000.

[31] NEA-OECD, Exposure to Radiation from Natural Radioactivity in Building Materials, NEA Group of Experts, OECD, Paris, 1979.

[32] S. Righi, L. Bruzzi, Natural radioactivity and radon exhalation in building materials used in Italian dwellings, J. Environ. Radioact. 88 (2006) 2, pp. 158–170.
DOI: 10.1016/j.jenvrad.2006.01.009

[33] Durridge Company Inc., RAD8 Radon + Thoron Monitor – User Manual, Durridge Co., Billerica, 2025.

[34] P. Tuccimei, M. Moroni, S. Di Norcia, Simultaneous determination of ^{222}Rn and ^{220}Rn exhalation rates from building materials used in Central Italy with accumulation chambers and a continuous solid state alpha detector: influence of particle size, humidity and precursors concentration, Appl. Radiat. Isot. 64 (2006) 2, pp. 254–263.
DOI: 10.1016/j.apradiso.2005.07.016

[35] M. Abo-Elmagd, Radon exhalation rates corrected for leakage and back diffusion–evaluation of radon chambers and radon sources with application to ceramic tile, J. Radiat. Res. Appl. Sci. 7 (2014) 4, pp. 390–398.
DOI: 10.1016/j.jrras.2014.07.001

[36] F. Caridi, L. Pistorino, F. Minissale, G. Paladini, M. Guida, S. Mancini, D. Majolino, V. Venuti, ^{222}Rn exhalation rate of building materials: comparison of standard experimental protocols and radiological health hazard assessment, Appl. Sci. 15 (2025) 14, pp. 8015.
DOI: 10.3390/app15148015

[37] V. Olivetti, A. J. Cyr, P. Molin, C. Faccenna, D. E. Granger, Uplift history of the Sila Massif, southern Italy, deciphered from cosmogenic ^{10}Be erosion rates and river longitudinal profile analysis, Tectonics 31 (2012).
DOI: 10.1029/2011TC003037

[38] G. Forestieri, M. A. De Buergo, Relationships between petrophysical and mechanical properties of certain calcarenites used in building, Geotech. Geol. Eng. 39 (2021), pp. 5021–5040.
DOI: 10.1007/s10706-021-01810-2

[39] F. Caridi, G. Paladini, S. Marguccio, M. D'Agostino, A. Belvedere, V. Crupi, D. Majolino, V. Venuti, Radioactivity content in construction materials of assets of particular historical-artistic interest, Proc. of the 2023 IMEKO TC4 Int. Conf. on Metrology for Archaeology and Cultural Heritage, Rome, Italy, 19-21 October 2023, 5 pp.
DOI: 10.21014/tc4-ARC-2023.163

[40] M. Degerlier, Assessment of natural radioactivity and radiation hazard in volcanic tuff stones used as building and decoration materials in the Cappadocia region, Turkey, Radioprotection 48 (2013), pp. 215–229.
DOI: 10.1051/radiopro/2012041

[41] F. Caridi, G. Paladini, S. Marguccio, A. Belvedere, M. D'Agostino, (+ 4 more authors), Evaluation of radioactivity and heavy metals content in a basalt aggregate for concrete from Sicily, southern Italy: a case study, Appl. Sci. 13 (2023) 8, pp. 4804.
DOI: 10.3390/app13084804

[42] M. Karaboue, D. Berritto, G. V. Lacasella, Council Directive 2013/59/Euratom of 5 December 2013 laying down basic safety standards for protection against the dangers arising from exposure to ionising radiation: medico-legal and legal-comparative study, Clin. Ter. 175 (2024) 5.
DOI: 10.7417/ct.2024.5127

[43] World Health Organization, WHO Indoor Radon: A Public Health Perspective, World Health Organization, Geneva, 2009.

[44] US Environmental Protection Agency, Exposure Factors Handbook, US Environmental Protection Agency, Washington DC, 2011.

[45] H. R. Rollinson, Using Geochemical Data: Evaluation, Presentation, Interpretation, Routledge, London, 2014.

[46] P. W. O. Hoskin, Trace-element composition of hydrothermal zircon and the alteration of Hadean zircon from the Jack Hills, Australia, Geochim. Cosmochim. Acta 69 (2005) 3, pp. 637–648.
DOI: 10.1016/j.gca.2004.07.006